On the application of strong thermoplastic–thermoset interactions for developing advanced aerospace-composite joints

Quan, Dong; Ma, Yannan; Yue, Dongsheng; Liu, Jiaming; Xing, Jun; Zhang, Mingming; Alderliesten, René; Zhao, Guoqun

DOI
10.1016/j.tws.2023.110671

Publication date
2023

Document Version
Final published version

Published in
Thin-Walled Structures

Citation (APA)
Quan, D., Ma, Y., Yue, D., Liu, J., Xing, J., Zhang, M., Alderliesten, R., & Zhao, G. (2023). On the application of strong thermoplastic–thermoset interactions for developing advanced aerospace-composite joints. *Thin-Walled Structures*, *186*, Article 110671. https://doi.org/10.1016/j.tws.2023.110671

Thin-Walled Structures 186 (2023) 110671

Contents lists available at ScienceDirect

Thin-Walled Structures

journal homepage: www.elsevier.com/locate/tws

On the application of strong thermoplastic–thermoset interactions for developing advanced aerospace-composite joints

Dong Quan [a], Yannan Ma [a], Dongsheng Yue [a], Jiaming Liu [a], Jun Xing [b], Mingming Zhang [b], René Alderliesten [c], Guoqun Zhao [a,*]

[a] Key Laboratory for Liquid-Solid Structural Evolution and Processing of Materials (Ministry of Education), Shandong University, China
[b] College of Environment and Safety Engineering, Qingdao University of Science and Technology, China
[c] Department of Aerospace Structures and Materials, Delft University of Technology, Netherlands

ARTICLE INFO

Keywords:
Composite joint
Thermoplastic–thermoset interaction
Co-curing joining
Fracture behaviour

ABSTRACT

In this study, an aerospace thermosetting composite was co-curing joined by Polyether-ether-ketone (PEEK) and Polyethylenimine (PEI) films, with an aim of developing advanced composite joints. The semi-crystalline PEEK films were surface activated upon a UV-irradiation technique to obtain a strong film–composite interface, while the amorphous PEI films could be directly used. The fracture behaviour of the composite joints was evaluated and compared with benchmark aerospace adhesive joints. The experimental results proved remarkable mode-I and mode-II fracture resistance of the PEEK co-cured joints at 22 °C and 130 °C, while the PEI co-cured joints exhibited excellent mode-I fracture resistance at 22 °C and mode-II fracture resistance in both testing temperature cases. Extensive elongation, tearing and fracture of the PEEK/PEI plastics were proved to be the main mechanisms for toughness enhancement. Overall, this work had successfully demonstrated the effectiveness of developing advanced composite joints via a co-curing process using high-performance thermoplastic films.

1. Introduction

Carbon fibre reinforced thermosetting composites had been widely used in aviation industries over the last two decades [1,2], that significantly reduced the aircraft weight and enhance their structural integrity. This resulted in significantly increasing usage of aerospace composite structures that were joined together by multi-components [3,4]. Accordingly, the development of effective joining techniques for composite parts became critical for aviation safety. Adhesive bonding is known as an ideal method for composite joining, due to its possibility to achieve low weight construction, high bonding strength and relatively uniform stress distribution [5–7]. For these reasons, adhesive bonding is one of the major joining techniques for aircraft assembly.

The majority of aerospace adhesives used epoxy resins as matrix owing to the high mechanical properties and good chemical resistance [8]. Due to the critical demand in aviation safety, these aerospace epoxy adhesives are typically supplied as one-component to ensure a good bonding quality and performance, i.e. this can avoid voids, inadequate mixing and non-stoichiometric weighting during the preparation process of two-component adhesives. However, this brings in a shortcoming that the aerospace adhesives possess a certain shelf life and require low temperature conditions for transportation and storage. For example, the shelf life of typical aerospace film adhesives, such as FM300 from Solway and AF163-2 from 3M is 12 months at −18 °C and 4 months at −4 °C. The shelf life significantly reduces to less than 20 days if the adhesives are stored at room temperature [9]. Another considerable shortcoming of epoxy resins is that their fracture toughness and crack resistance are low, due to the highly cross-linked molecular structures of the epoxy resins [10]. For this reason, different types of toughening additives are normally used to enhance the crack resistance of epoxy [11,12], which significantly increases the cost of the adhesives. Additionally, even though the aerospace adhesives are typically intensively toughened [13,14], fracture failure is still the major failure mode of composite adhesive joints in aerospace components. For the above reasons, it is appealing to propose substitutes of epoxy adhesives for the joining of composite materials, who possess unlimited shelf life and excellent fracture toughness.

High-performance engineering thermoplastics, such as Polyetherimide (PEI), Polyphenylene sulphide (PPS) and Polyether ether ketone (PEEK) etc. exhibited excellent fracture toughness, high thermal stability and unlimited shelf life. Accordingly, there is a high potential of utilising these TP materials for thermosetting composite joining, with a strong interface at the composite–thermoplastic interface being a critical condition. Recent studies on the interactions between thermoplastic films and epoxy resins had been comprehensively reviewed by Deng

* Corresponding author.
E-mail address: zhaogq@sdu.edu.cn (G. Zhao).

https://doi.org/10.1016/j.tws.2023.110671
Received 13 November 2022; Received in revised form 28 January 2023; Accepted 28 February 2023
Available online xxxx
0263-8231/

et al. [15]. The interacting mechanisms at the interfaces between epoxy resins and amorphous thermoplastics, including Polysulfone (PSU), Polyethersulfone (PES), Polyetherimide (PEI) and Polyamide (PA) had been discussed. In general, the epoxy resins and amorphous thermoplastic moleculars diffused into each other during the curing process, that generated an interdiffusion zone at their interfaces and formed strong bond [16,17]. Noteworthily, the majority of literatures utilised thermoplastic–epoxy interactions for co-curing a layer of thermoplastic onto the surfaces of carbon fibre/epoxy composites [15,18]. This allowed welding to be conducted to join the carbon fibre/epoxy adherends by fusion bonding using the similar processes for joining thermoplastics and thermoplastic based composites [19,20]. While these studies proved that good thermoset/thermoplastic interactions were feasible, one can hardly find any study on utilising thermoplastics for the joining of aerospace thermosetting composites. Our recent study proposed to replace structural film adhesives by a layer of carbon fibre reinforced PEEK (CF/PEEK) for the co-cure joining of epoxy-based aerospace composites [21]. The experimental results revealed significant potential and benefit of utilising thermoplastic materials for co-cure joining of thermosetting composites, i.e. remarkable improvements in the mechanical properties, fracture resistance and thermal stability of the composite joints at both of room temperature and high temperature were obtained [21]. Accordingly, it is appealing to further develop this technique by investigating the structural integrity of aerospace composite components that was co-cure joined by various types of advanced thermoplastic materials.

In this study, semi-crystalline PEEK films and amorphous PEI films with different thicknesses were used as joining agent for the co-cure joining of an aerospace thermosetting composite, with an aim of developing advanced composite joints. An UV-irradiation treatment was carried out to the PEEK films to promote their surface polarities and activities, and hence to form a strong interaction/bond at the PEEK-thermosetting interface. No surface treatment was performed to the PEI films, as they had good miscibility with thermosetting resins [15]. The effects of the materials, thicknesses and surface activities of the thermoplastic films on the fracture resistance of the co-cured composite joints were studied. Composite joints co-cure bonded by a commercial aerospace film adhesive were also prepared as benchmark. The fracture performance and mechanisms of the co-cured joints under mode-I and mode-II loading conditions were studied, with excellent fracture toughness being observed for the thermoplastic co-cure joined thermosetting composite joints.

2. Experimental

2.1. Materials

The thermosetting composite was based on a unidirectional prepreg, Hexply F6376C-HTS (12K)-5%–35% supplied by HEXCEL Composites (UK). The reinforcement was Tenax-E HTS45 standard modulus fibres (TOHO TENAX Europe GmbH) with a high tenacity, and the thermosetting resin was Hexply F6376 thermoplastic-toughened epoxy resin. Semi-crystalline PEEK films with a thickness of 100 μm, 200 μm, 250 μm were APTIVE 1000 series from Victrex (UK). Amorphous PEI films with a thickness of 90 μm, 175 μm and 250 μm were supplied by LITE (Germany). The PEEK and PEI films were selected as both of them were widely used for aerospace applications. Additionally, the PEEK represented a semi-crystalline polymer that possessed poor surface activity and outstanding mechanical performance and environmental resistance, while PEI was an amorphous polymer that exhibited excellent interface adhesion with the aerospace composite materials and relatively poorer mechanical properties and environmental resistance than semi-crystalline PEEK. The benchmark aerospace adhesive was FM300 from Solvay (UK), which was one of the most widely used and well-commercialised structural adhesives for the aviation industry. This was a film adhesive in 146 g/m^2 areal weight that was supported by random distributed thermoplastic non-woven fibres.

2.2. Composite joint manufacturing

Fig. 1 presents the procedures for the preparation of the composite joints that were co-cure joined by the PEEK and PEI films. Since the surface polarity of PEEK films was inherently low, both sides of the PEEK films were UV-irradiated for 10 s prior to the laminate layup (see Fig. 1(a) and (b)). The UV-irradiation treatment that was applied to the PEEK surfaces were the same as used in our previous studies [22,23], which could significantly promote the epoxy–PEEK interface adhesion, and additional information can be found in [22,23]. No special surface treatment apart from degreasing and cleaning by isopropanol was needed for the PEI films, as they could form an interdiffusion zone with the epoxy during the composite curing process. Following the surface treatment, the PEEK and PEI films were placed between two prepreg layups with a stacking sequence of $[0_{16}]$ (see Fig. 1(c)). A piece of thin PTFE foil was also placed above one side of the thermoplastic films during the hand layup process. The PTFE foil possessed extremely low adhesion with the laminate matrix, and hence can serve as crack insert for the following fracture tests. The composite joint assemble was then cured in an autoclave using a schedule of 0.4 MPa at 180 °C for 90 mins, during which a 200 mbar vacuum pressure was applied to the joint assemble (see Fig. 1(d)). A diamond grinding machine was then used to cut the composite joints into individual specimens for the fracture tests (see Fig. 1(e)–(g)). Composite joints co-cured by the aerospace adhesive FM300 were also prepared using the same procedure as a benchmark. Additionally, composite laminate, i.e. without using adhesive or thermoplastic films for the joining in Fig. 1(c), was also manufactured as a reference. In the rest part of this paper, the composite joints that are co-cure joined by the PEEK films, the PEI films and the FM300 adhesive are named as PEEK-CoJoints, PEI-CoJoints and FM300-CoJoints, respectively.

2.3. Testing and characterisation

The fracture toughness of the composite joints under mode-I and mode-II loading conditions was evaluated using a DCB (double cantilever beam) test [24] and a ENF (end notched flexural) test [25], respectively. Fig. 1(f) and (g) schematically show the loading setup and specimen dimensions of the mode-I and mode-II fracture tests, respectively. The DCB and ENF tests were performed in a universal testing machine at a loading rate of 2 mm/min and 0.5 mm/min, respectively. It is worthy to mention that the loading rate within a range of 0.5–2 mm/min satisfied a quasi-static loading condition, and it had none effect on the measured values of the mode-I and mode-II fracture energies. A smaller loading rate for the ENF tests was to facilitate the precise monitoring of the location of the mode-II crack tip, which was more difficult to be identified than the mode-I crack tip. The tests were carried out at a low temperature of 22 °C and a high temperature of 130 °C within a temperature chamber. The location of the crack front was recorded using a high resolution digital camera during the fracture tests. Three specimens were tested in each case.

The fracture energy under mode-I loading (G_{IC}) was calculated based on a modified beam theory specified in [24]:

$$G_{IC} = \frac{3P\delta}{2b(a+|\Delta|)} \tag{1}$$

where P is the value of the load, a is the length of the crack, b is the width of the DCB specimen and δ is the displacement at the loading point.

The fracture energy under mode-II loading (G_{IIC}) was derived based on a CC (compliance calibration) theory defined in [25]:

$$G_{IIC} = \frac{3mP^2a^2}{2b} \tag{2}$$

where m is the coefficient of the CC test, which was measured by performing the CC tests on the ENF specimens [25].

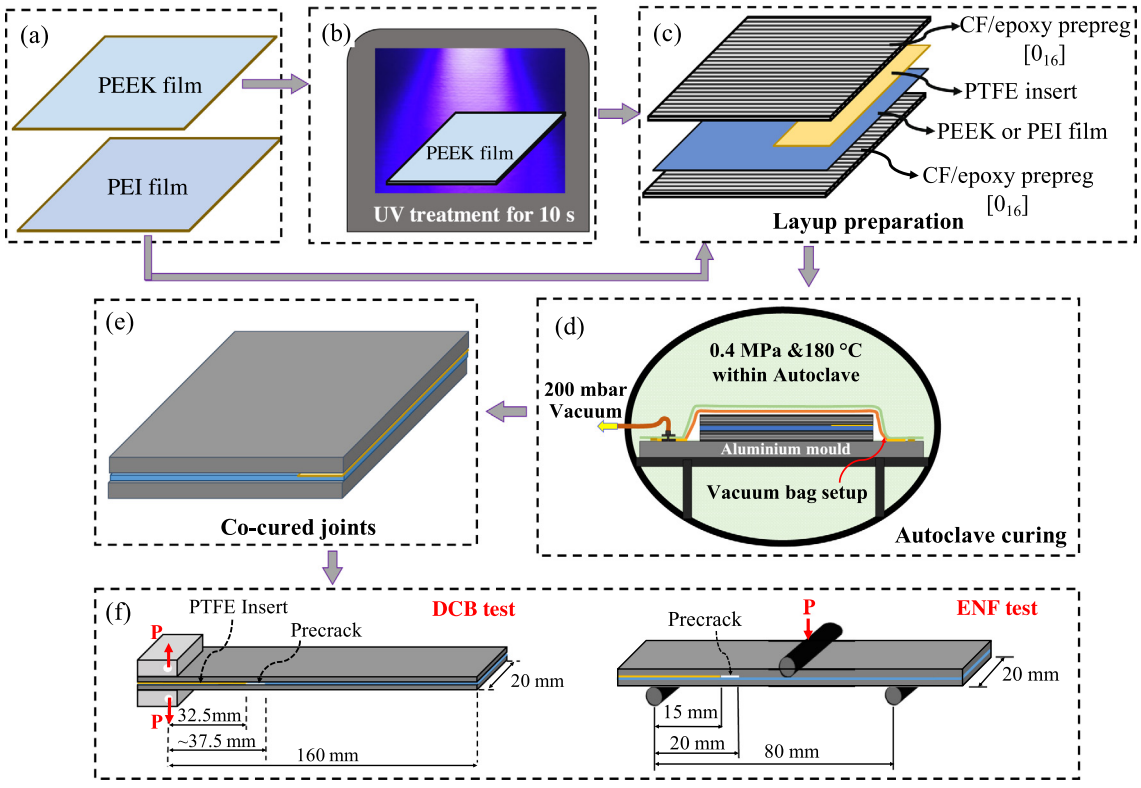

Fig. 1. The procedure for the composite joint manufacturing and specimen preparation.

The cross-section of the co-cured composite joints was analysed using a SEM (JEOL JSM-7500F) to investigate the morphology at the thermoplastic–composite interface. To provide a better contrast, the polished surface of the specimen was etched by a drop of N-Methyl-2-pyrrolidone (NMP) (about 1–2 ml) and then washed by running water. The fracture surfaces of the composite joints were imaged using the SEM and a laser microscope (KEYENCE VK-X1000). Prior to the SEM imaging, the surfaces of the specimens were sputtered by gold to create a 5 nm thick electric-conductive layer.

3. Experimental results

3.1. Interface morphology

To ensure good structural performance of co-cured composite joints, it is critical to obtain strong interfaces between the PEEK/PEI films and the composite based on epoxy resin. In this study, the PEI films were amorphous thermoplastic that possessed a high miscibility with epoxy resins [16,17]. In the course of the joint curing, the epoxy resin and the PEI molecules diffused into each other to a certain distance at the interface, that was followed by a phase separation at certain reaction temperature [26]. Fig. 2(a)–(c) present the morphology of the interdiffusion region at the PEI-epoxy interface of the PEI-CoJoints. Obviously, extensive mutual interdiffusion between PEI and epoxy took place during the laminate curing process, that was indicated by the presence of numerous epoxy spheres at the side of the PEI film (Fig. 2(b)) and PEI spheres at the side of the epoxy composite (Fig. 2(c)). The interdiffusion layer at the PEI-epoxy interface possessed an average thickness of 30.3 ± 7.3 μm, that had provided good joining strength between the PEI films and the laminate, as will be shown later on.

As expected, a distinct PEEK-epoxy interface was observed within the PEEK-CoJoints (see Fig. 2(d)). This was mainly due to the semi-crystalline structure of the PEEK molecule, which prevent the PEEK-epoxy interdiffusion at the interface. It should also be noted that PEEK possessed very low reactivity, small surface energies and poor polarities, that resulted in poor adhesion with epoxies. Accordingly, to develop PEEK-CoJoints with good mechanical performance, proper surface treatment to the PEEK films was required to provide strong bonds at the epoxy–PEEK interface. The UV-irradiation treatment that was applied in this study (see Section 2.3) utilised the high power of the UV-light to break the C–C bond of the PEEK molecules, that was followed by the creation of functional O–C=O, C=O and C–O groups [23,27]. The addition of these oxygen groups on the PEEK surfaces significantly promoted their chemical reaction with the epoxy matrix during the curing process of the composite joints. Subsequently, strong bonding between the PEEK and the epoxy was obtained (that was approved in Sections 3.2.3 and 3.3.3), even though no mutual interdiffusion occurred between PEEK and epoxy.

3.2. The fracture behaviour under mode-I loading

3.2.1. Mode-I fracture of the reference laminate and benchmark adhesive joints

Fig. 3 presents the results of the DCB tests for the reference laminate and their adhesive joints bonded by FM300. Overall, a much better fracture resistance under mode-I loading was observed for the FM300-CoJoints than the reference laminate in both cases of the testing temperature. For example of the testing results at 22 °C, the peak load for the FM300-CoJoints was 136 N, that was approximately two times of the value for the reference laminate, see Fig. 3(a). Accordingly, the FM300-CoJoints possessed much higher mode-I fracture energies (G_{IC}) than the reference laminate, see Fig. 3(b) and (c). An average value of 362 J/m^2 and 1353 J/m^2 was obtained for G_{IC} of the reference laminate and the FM300-CoJoints at 22 °C, respectively. The fracture resistance of the reference laminate under mode-I loading had been slightly improved while the testing temperature was increased to 130 °C, as shown by the increased fracture propagation load in Fig. 3(a) and G_{IC} values in Fig. 3(b) and (c). G_{IC} of the reference laminate at 130 °C was 545 J/m^2, that was 51% higher than the value at 22 °C.

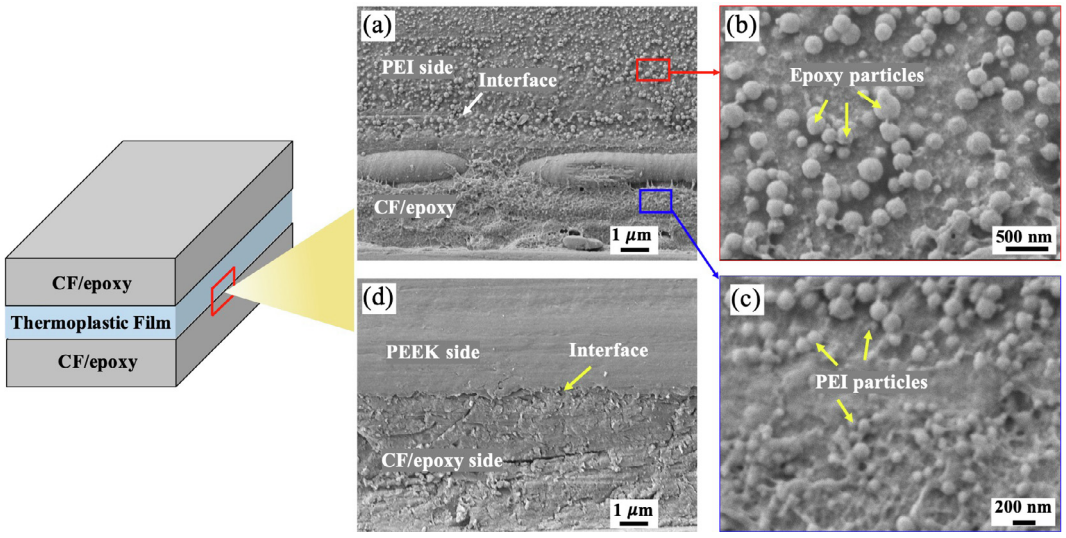

Fig. 2. The morphology of thermoplastic–epoxy interfaces within the composite joints: (a)–(c) are for the PEI–epoxy interface and (d) is for the PEEK–epoxy interface.

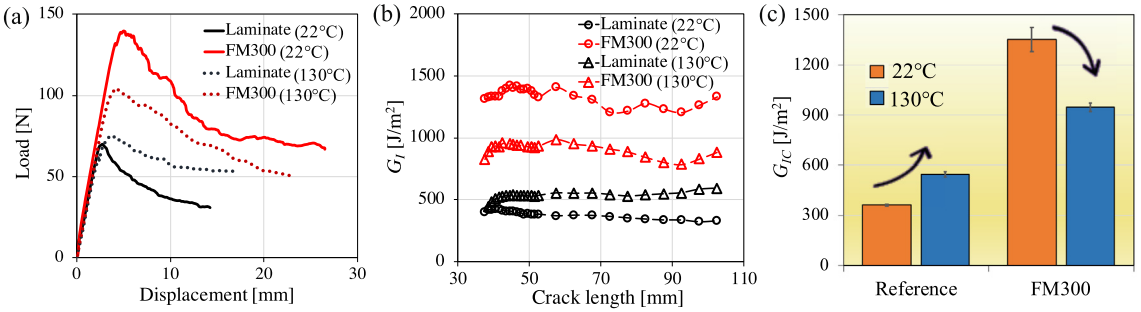

Fig. 3. The results of the mode-I DCB fracture tests of the reference laminate and their FM300-CoJoints: (a) the load–displacement curves, (b) the *R*-curves and (c) the mode-I fracture energies.

Opposite change in the mode-I fracture performance was observed for the FM300-CoJoints as the testing condition increasing from 22 °C to 130 °C, i.e. G_{IC} of the FM300-CoJoints declined from 1353 J/m^2 to 946 J/m^2 (by 43%).

Fig. 4 presents the photographs of the DCB specimens during the testing, for showing the fibre bridging phenomenon at the wake of the crack. By carefully comparing Fig. 4(a) and (b) with Fig. 4(c) and (d), one can see that more intensive fibre bridging took place at 130 °C than at 22 °C for both of the reference laminate and the FM300-CoJoints. The bridging fibres for the reference laminate were carbon fibres, while the bridging fibres observed in Fig. 4(b) and (d) were the thermoplastic non-woven within the FM300 adhesives. Typical SEM micrographs of the DCB fracture surfaces for the reference laminate and the FM300-CoJoints are presented in Fig. 5. By comparing Fig. 5(a) and (b), it was observed that extensively more carbon fibres delaminated and broke at 130 °C than at 22 °C. The breakage of more carbon fibres resulted in extra energy dissipation, and hence a higher G_{IC} at 130 °C, as shown in Fig. 3. Many randomly orientated thermoplastic fibres appeared on the surfaces of the fractured FM300-CoJoints in Fig. 5(c) and (d), indicating fibre debonding and bridging being the main failure mechanisms. However, unlike the carbon fibres, the thermoplastic non-woven had a typically poor adhesion/interaction with the laminate epoxy matrix, evidenced by the smooth surfaces of the majority of the thermoplastic fibres. This meant that the required forces for the debonding of the thermoplastic fibres during the DCB tests were relatively low. By increasing the testing condition from 22 °C to 130 °C, the epoxy matrix and the thermoplastic fibres became soft and their interface adhesion further decreased. This negatively affected the effectiveness of the thermoplastic fibre debonding and bridging mechanisms for energy dissipation, and led to considerable drops in G_{IC}, see Fig. 3

3.2.2. Mode-I fracture of the PEEK/PEI-Cojoints

Fig. 6(a)–(c) presents the results of the DCB tests of the PEEK/PEI-CoJoints that were tested at 22 °C. The curves for the reference laminate and the FM300-CoJoints were included for the comparison purpose In Fig. 6 and the following sections of this paper, the joints co-cured by the PEEK/PEI films was referred to as the polymer type and its thickness in μm, e.g. PEI175 indicates the PEI-CoJoints that were co-cure joined by 175 μm thick PEI films. The PEEK-CoJoints exhibited a stick–slip crack propagation behaviour for the mode-I fracture tests at 22 °C. The peak loads corresponding to the crack arrest points of the PEEK-CoJoints were slightly higher than that of the FM300-CoJoints, as shown in Fig. 6(a). This resulted in significantly varied fracture toughness of the PEEK-CoJoints in Fig. 6(c). Additionally, the effect of the PEEK thickness was trivial on the fracture resistance of the PEEK-CoJoints under mode-I loading. A stable crack propagation took place to the PEI-CoJoints, and the crack propagation loads were lower than that of the FM300-CoJoints and higher than that of the reference laminate, see Fig. 6(b). Accordingly, the *R*-curves of the PEI-CoJoints fell between those of the FM300-CoJoints and the reference laminate in Fig. 6(c).

The experimental results of the mode-I fracture tests for the composite joints at a testing temperature of 130 °C are presented in Fig. 6(d)–(f). During the DCB tests at 130 °C, the initial stable crack propagation was always followed by a jump (rapid crack propagation) or dynamic failure of the entire specimens for the PEEK-CoJoints, while crack propagation of the PEI-CoJoints exhibited a stick–slip manner.

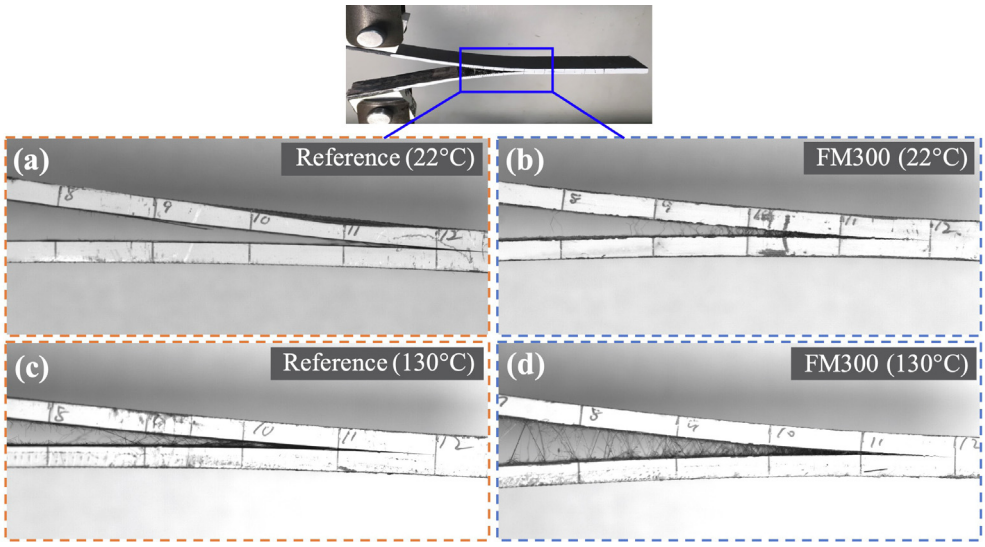

Fig. 4. The fibre bridging phenomenon at the wake of the crack during the DCB tests of the reference laminate and the FM300-CoJoints.

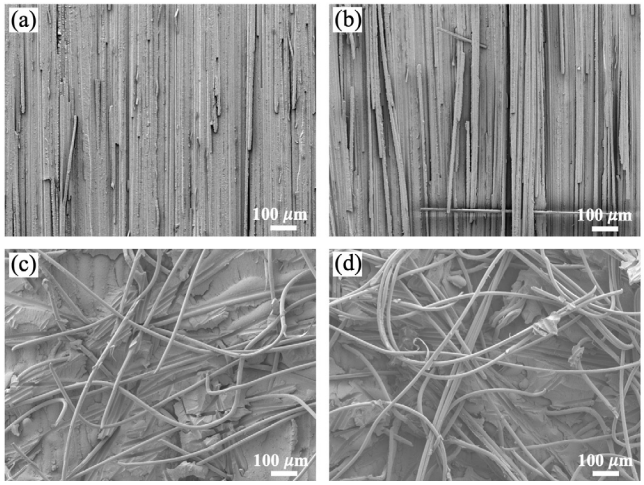

Fig. 5. Typical SEM images of the mode-I fracture surfaces of the reference laminate and the FM300-CoJoints: (a) and (b) is for the reference laminate at 22 °C and 130 °C, respectively; (c) and (d) is for the FM300-CoJoints at 22 °C and 130 °C, respectively.

This explained why a limited number of values were recorded on the *R*-curves of the PEEK-CoJoints and PEI-CoJoints in Fig. 6(f). Obviously, the PEEK-CoJoints showed remarkable mode-I fracture resistance at 130 °C, i.e. their crack propagation loads and corresponding *R*-curves were significantly higher than that of the FM300-CoJoints, see Fig. 6(d) and (f). The crack propagation of the PEI-CoJoints changed from a stable mode to a stick–slip mode as the temperature of the DCB tests increasing from 22 °C to 130 °C. Additionally, the peak loads on the load–displacement curves of the PEI-CoJoints were much higher than the crack propagation loads of the FM300-CoJoints at 130 °C. Consequently, the *R*-curves of the PEI-CoJoints were greater than that of the FM300-CoJoints and the reference laminates in Fig. 6(f). However, the fracture performance of the PEEK-CoJoints was still superior when compared with the PEI-CoJoints.

Table 1 summarises the values of G_{IC} of the composite joints that were measured by the DCB tests. The values of G_{IC} for the reference laminate and their FM300-CoJoints were 362 J/m^2 and 1353 J/m^2, respectively at 22 °C. The PEEK-CoJoints possessed more or less the same G_{IC} as the FM300-CoJoints at 22 °C, if the standard deviation was considered. However, G_{IC} of the composite joints considerably dropped by over 40% upon replacing the FM300 adhesives with the PEI films.

Table 1
The mode-I fracture energies, G_{IC} of the co-cured composite joints and the reference laminate.

Items	G_{IC} at 22 °C (J/m^2)	G_{IC} at 130 °C (J/m^2)
Laminate	362 ± 17	545 ± 4
FM300	1353 ± 25	946 ± 71
PEEK100	1311 ± 137 (−3%)	4312 ± 375 (356%)
PEEK200	1505 ± 80 (11%)	3671 ± 387 (288%)
PEEK250	1531 ± 178 (13%)	3868 ± 198 (309%)
PEI90	552 ± 41 (−59%)	1255 ± 337 (33%)
PEI175	781 ± 25 (−42%)	1860 ± 147 (97%)
PEI250	760 ± 75 (−44%)	1727 ± 10 (83%)

In specific, the average value of G_{IC} was calculated to be 552 J/m^2 for the PEI60 joints at 22 °C, and it increased to 781 J/m^2 for the PEI175 joints, and then remained essentially the same for the PEI250 joints. Noteworthily, these values were still much higher than that of the reference laminate. Encouragingly, both of the PEEK-CoJoints and PEI-CoJoints possessed much higher G_{IC} than the FM300-CoJoints at 130 °C, with more remarkable mode-I fracture resistance being proved for the PEEK-CoJoints. For instance, G_{IC} of the PEEK100 joints at a testing temperature of 130 °C was 356% higher than that of the FM300-CoJoints. A 33% increase in G_{IC} at 130 °C was obtained upon replacing the FM300 adhesive with 60 μm PEI films for the composite co-cure joining, while this value had significantly increased to 97% and 93% as the thickness of the PEI increased to 175 μm and 250 μm, respectively.

3.2.3. Mode-I fractography of PEEK/PEI-Cojoints

Fig. 7 presents typical photographs of the fracture surfaces for the co-cured joints under the mode-I loading condition. From Fig. 7(a) and (b), one can see that the two surfaces of the fractured PEEK-CoJoints were characterised with extensively fractured PEEK resins, with some of the resin-sparse locations appeared in a black colour. Additionally, the insert images showed that a very thin layer of PEEK resin appeared on the resin-sparse locations. The phenomena proved that the PEEK-CoJoints fractured cohesively inside the PEEK layers under the mode-I loading at both of 22 °C and 130 °C. A thin-layer cohesive failure took places to the PEI-CoJoints at 22 °C, i.e. most of the PEI film remained on one surface of the fractured specimens, while the opposite fractured surface was attached with a tiny layer of PEI resin, as shown in Fig. 7(c). As the temperature increased from 22 °C to 130 °C, the failure behaviour of the PEI-CoJoints alternated from a thin-layer cohesive mode to the peeling-out of carbon fibres from surrounding resins. This was evidenced by the presence of numerous

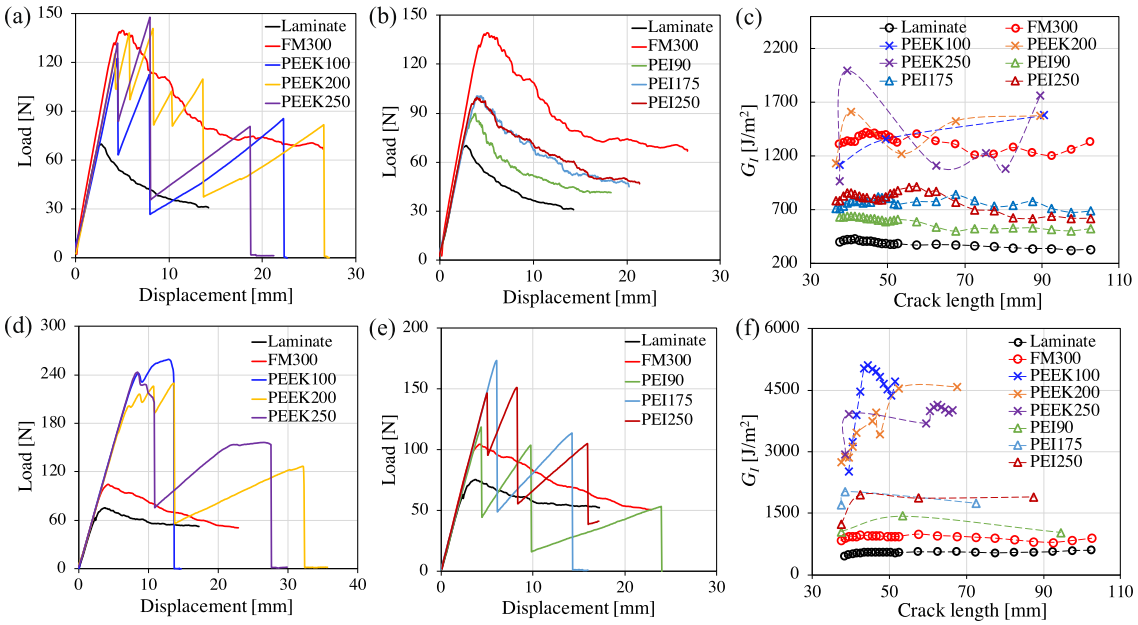

Fig. 6. The load–displacement curves and corresponding *R*-curves from the DCB tests of the PEEK/PEI-CoJoints: (a-c) at 22 °C and (d-f) at 130 °C.

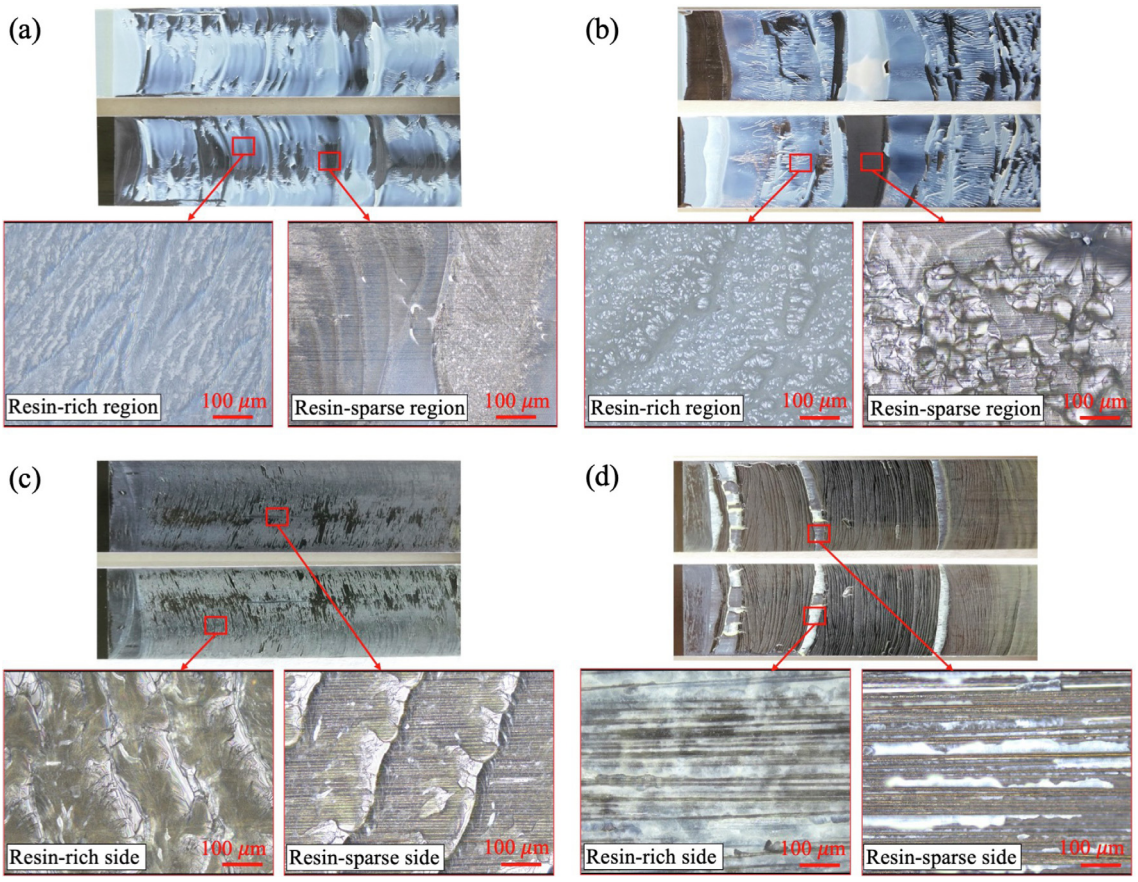

Fig. 7. Representative photos for the fracture surfaces of the DCB specimens of (a) PEEK-CoJoints at 22 °C, (b) PEEK-CoJoints at 130 °C, (c) PEI-CoJoints at 22 °C and (d) PEI-CoJoints at 130 °C.

fibre printing on the resin-rich side and bare carbon fibres on the resin-sparse side. Another obvious observation from Fig. 7 was that the PEEK and PEI resins appeared differently on the fracture surfaces for 22 °C and 130 °C, that can be further revealed by analysing the SEM micrographs of the fracture surfaces.

Fig. 8 shows typical SEM micrographs of the fractured DCB specimens for the PEEK/PEI-CoJoints. Evidence of significant plastic deformation and damage to the PEEK resins was observed on the fracture surfaces of the PEEK-CoJoints for both of the 22 °C and 130 °C cases, see Fig. 8(a) and (b). Additionally, more prominent deformation,

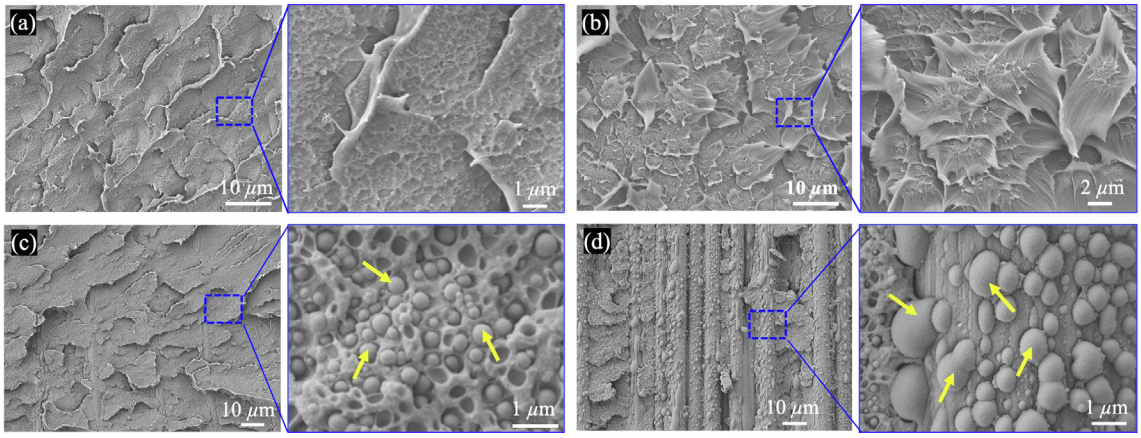

Fig. 8. Representative micrographs of the mode-I fracture surfaces for the co-cured composite joints: (a) and (b) are for the PEEK-CoJoints at 22 °C and 130 °C, respectively; (c) and (d) are for the PEI-CoJoints 22 °C and 130 °C, respectively.

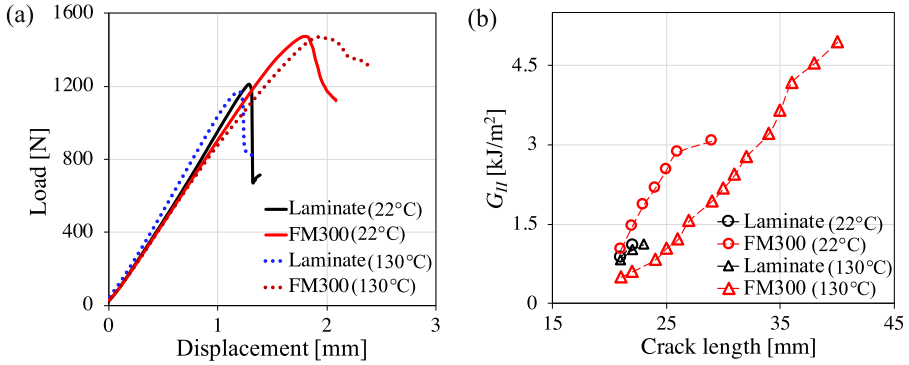

Fig. 9. The load–displacement curves and corresponding mode-II *R*-curves of the reference laminate and FM300-CoJoints.

elongation and tearing of the PEEK films were observed for the 130 °C cases. This was attributed to the thermal softening of the PEEK layers at the high temperature, which lead to considerable increases in the ductility and decreases in the strength and stiffness. The good ductility of the PEEK layer at 130 °C could significantly blunt the crack tip inside the PEEK layers during the mode-I crack growth, that subsequently relieved the stress concentration at the crack tip vicinity and dissipated significantly more energy. This explained why more intensive damage characteristics were observed for the PEEK films at 130 °C, which resulted in the very high G_{IC} values of the PEEK-CoJoints in Table 1. The PEI-epoxy interdiffusion layer also underwent considerable plastic deformation and failure at 22 °C for the PEI-CoJoints, as shown by Fig. 8(c). Additionally, the presence of debonded particles and holes on the fracture surfaces indicates significant particle debonding and plastic void growth mechanisms during the fracture process [10]. Fig. 8(d) shows representative SEM micrographs of the mode-I fracture surfaces for the PEI-CoJoints at 130 °C. The fracture surfaces were characterised with many carbon fibres, indicating the debonding of carbon fibres from surrounding resins during the mode-I crack propagation . Moreover, a significant number of hemispheric PEI particles were observed on the debonded carbon fibres These PEI particles led to significant crack pining mechanism during the mode-I fracture propagation, which consumed additional fracture energy. This, together with the thermal softening effect contributed to the notable increases in G_{IC} of the PEI-CoJoints as the testing temperature had been increased from 22 °C to 130 °C, see Table 1.

3.3. The fracture behaviour under mode-II loading

3.3.1. Mode-II fracture of the reference laminate and benchmark adhesive joints

The load–displacement curves and corresponding *R*-curves of the reference laminate and benchmark adhesive joints under mode-II loading are shown in Fig. 9. Noteworthily, the reference laminate exhibited a dynamic failure during the mode-II ENF tests. This explained why only a limited number of values were recorded for the reference laminate in Fig. 9(b). No significant difference in the load–displacement responses and mode-II *R*-curves was observed for the reference laminate at 22 °C and 130 °C, indicating a good thermal resistance of the reference laminate under mode-II fracture failure. Similarly, the peak loads on the load–displacement curves for the FM300-CoJoints at 22 °C and 130 °C were also approximately the same, as shown in Fig. 9(a). Additionally, significant "rising" mode-II *R*-curves were observed for the FM300-CoJoints for both of 22 °C and 130 °C cases, see Fig. 9(b). This typically means that the fracture process zone in front of the crack tip extended in the length as the mode-II shearing load increased [28]. However, a dynamic failure took place to the FM300-CoJoints after the crack stably propagated for about 10 mm at 22 °C, while the crack grew stably for the FM300-CoJoints throughout the course of the ENF tests at 130 °C. This explained why no point was recorded on the *R*-curves at a crack length of above 30 mm for the FM300-CoJoints at 22 °C, see Fig. 9(b). Accordingly, the maximum values on the *R*-curves of the FM300-CoJoints was higher at 130 °C than at 22 °C. Nevertheless, it is worthy to mention that the *R*-curve values of the FM300-CoJoints

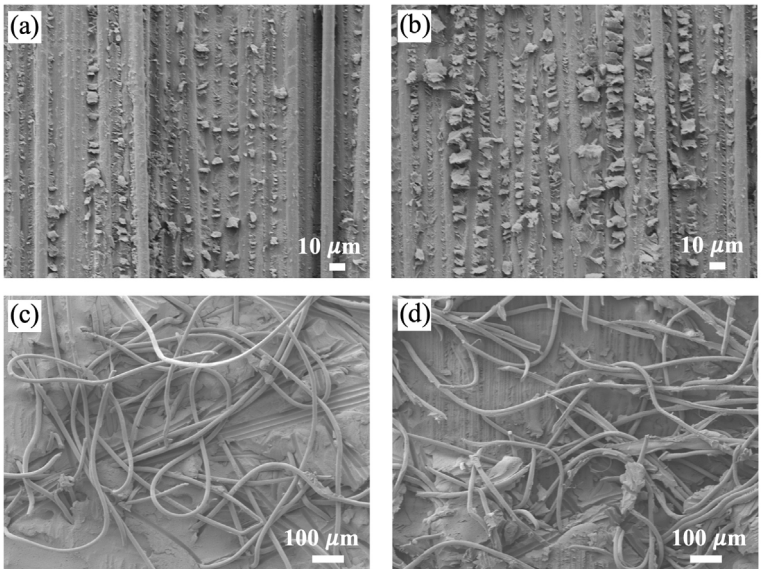

Fig. 10. Representative micrographs of the mode-II fracture surfaces of the reference laminate and the FM300-CoJoints: (a) and (b) is for the reference laminate at 22 °C and 130 °C, respectively; (c) and (d) is for the FM300-CoJoints at 22 °C and 130 °C, respectively.

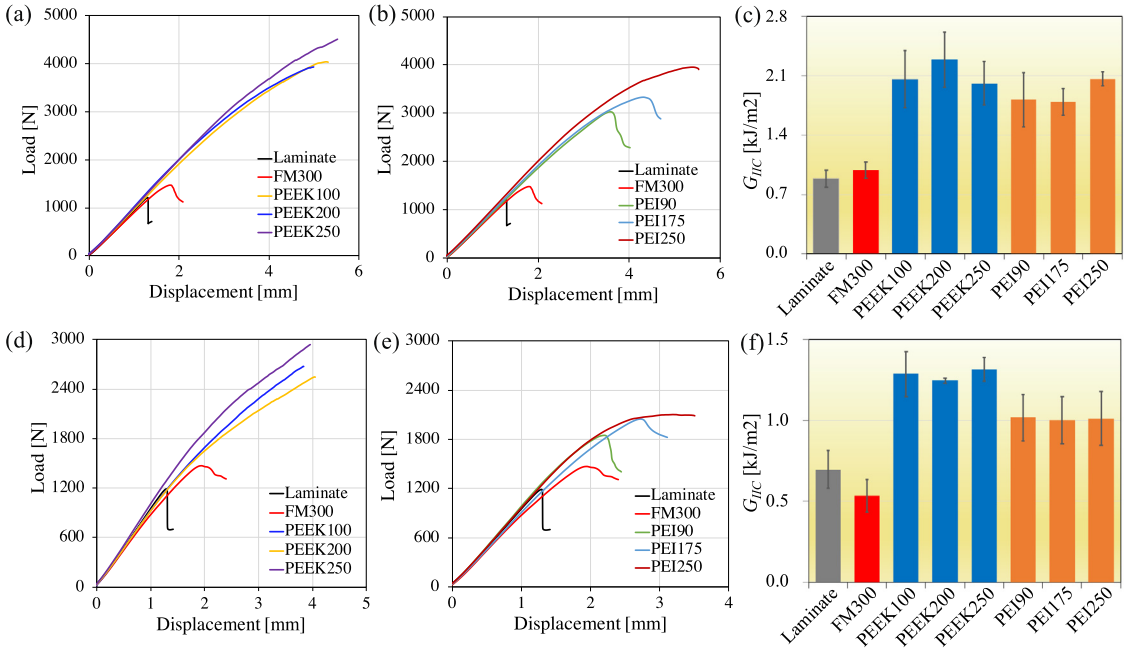

Fig. 11. The load–displacement curves and corresponding G_{IIC} from the ENF tests of the PEEK/PEI-CoJoints: (a-c) at 22 °C and (d-f) at 130 °C.

at 22 °C were much higher than that at 130 °C for a crack length less than 30 mm.

Fig. 10 shows representative SEM micrographs of the ENF fracture surfaces for the reference laminate and the benchmark adhesive joints. No obvious difference in the fracture surfaces at 22 °C and 130 °C was observed for the reference laminate, see Fig. 10(a) and (b). Delamination of the carbon fibres and shearing damage of the epoxy at the carbon fibre intervals were revealed to be the main failure mechanisms for the reference laminate. Similarly as the mode-I fracture, numerous thermoplastic fibres presented on the mode-II fracture surfaces of the FM300-CoJoints for both of the 22 °C and 130 °C cases, as can be seen in Fig. 10(c) and (d). This phenomenon indicated that the thermoplastic fibres debonded from the adhesive matrix and bridged the crack growth plane at the mode-II crack tip during the ENF tests [29].

3.3.2. *Mode-II fracture of the thermoplastic film co-cured joints*

Fig. 11(a), (b), (d) and (e) show the load–displacement curves that were obtained by the mode-II ENF tests on all the co-cured joints and the reference laminate. The curves for the reference laminate and the FM300-CoJoints were included for the comparison purpose. Unlike the typical load–displacement curves for the reference laminate, no drop in the load occurred on the curves for all the PEEK-CoJoints and the PEI250-CoJoints at both of 22 °C and 130 °C. This corresponded to an abnormal fracture failure mode of the ENF specimens for the thermoplastic film co-cured joints in all the cases, as schematically shown by Fig. 12(a). During the ENF tests, many sub-cracks were generated ahead of the crack tip without causing continuous propagation of the main crack (see Fig. 12(a)). This type of failure mode was caused by the high ductility and failure strength of the PEEK and PEI films under shear loading conditions. Noteworthily, the ENF tests had to been terminated

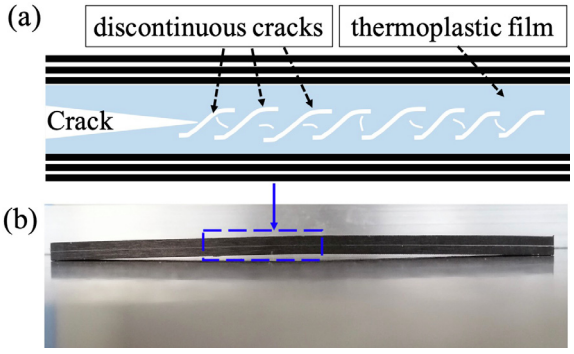

Fig. 12. (a) a schematic for showing the state of the mode-II crack front of the PEEK-CoJoints and (b) a tested PEEK-CoJoint specimen for showing the bending of the ENF specimens.

once the sub-cracks occurred at the loading position of the specimens in Fig. 1(g), otherwise complete fracture to the composite substrate of the ENF specimens would take place. Fig. 12(b) presents the side-view of an ENF specimen after the testing, which shows significant bending of the specimens after the test was terminated. This was because of the PEEK and PEI layers within the ENF specimens undertook extensive plastic deformation and damage under the mode-II loading, even though no complete separation took place to the ENF specimens. Overall, based on the load–displacement curves in Fig. 11, the PEEK/PEI-CoJoints exhibited remarkable resistance to mode-II fracture at both of 22 °C and 130 °C.

Owing to the irregular fracture mode of the ENF specimens for the PEEK/PEI-CoJoints, the mode-II fracture energy (G_{IIC}) was taken as the value at the instance of the sub-crack initiating in front of the precrack. The values of G_{IIC} for all the co-cured joints and the reference laminate are summarised in Fig. 11(c) and (f). Clearly, the PEEK/PEI-CoJoints had much greater G_{IIC} than the FM300-CoJoints and the reference laminate in both of the low temperature and high temperature cases. Additionally, the values of G_{IIC} for the PEEK-CoJoints were slightly higher than that of the PEI-CoJoints in both of the temperature cases. In specific, the values of G_{IIC} at 22 °C were determined to be 0.88 kJ/m^2 and 0.99 kJ/m^2 for the reference laminate and the FM300-CoJoints, respectively. At a testing condition of 130 °C, these values considerably declined to 0.70 kJ/m^2 and 0.54 kJ/m^2, respectively. For the PEEK-CoJoints, the PEEK thickness exhibited negligible effects on G_{IIC} at both of 22 °C and 130 °C, and G_{IIC} were measured to be varied between 2.0–2.3 kJ/m^2 at 22 °C and around 1.3 kJ/m^2 at 130 °C. These values were much greater than those for the FM300-CoJoints in all the corresponding cases. For the PEI-CoJoints, no statistically difference in G_{IIC} was observed by changing the thickness of the PEI films either. The measured values of G_{IIC} were around 1.8–2.1 kJ/m^2 at 22 °C and around 1.0 kJ/m^2 at 130 °C. These were also approximately 2 times of the values for the FM300-CoJoints in both cases.

3.3.3. *Mode-II fractography of the thermoplastic film co-cured joints*

Representative images of the mode-II fracture surfaces for the PEEK/PEI-Co-Joints are shown in Fig. 13. From Fig. 13(a) and (b), it was observed that the majority of the PEEK resin left on the lower side of the fractured ENF specimens, with a small portion of PEEK layer remained on the opposite side. This phenomenon indicated that a thin-layer cohesive failure took place to the PEEK-CoJoints under the mode-II loading, and explained why the PEEK thickness had negligible effects on G_{IIC} for both of the 22 °C and 130 °C cases. For the PEI-CoJoints, it was found that the entire PEI film was also attached on the lower side of the fracture surfaces, with numerous fibre prints being observed in both of the 22 °C and 130 °C cases, see Fig. 13(c) and (d). This means that the carbon fibres debonded from the surrounding PEI-epoxy interdiffused resin during the mode-II fracture process of the PEI-CoJoints. This type of failure mechanism led to non-obvious effect of the thickness of the PEI film on the PEI-CoJoints in Fig. 11(c) and (f).

Representative micrographs of the mode-II fracture surfaces for the PEEK/PEI-CoJoints are shown in Fig. 14. Numerous leaf-like characteristics presented on the fractured surfaces of the PEEK-CoJoints for both of the 22 °C and 130 °C cases, see Fig. 14(a) and (b). These “leaves” were the PEEK resins that undertook large-scale plastic deformation, tearing and damage while they were peel-off from the PEEK layers that remained on the opposite side of the fractured ENF specimens. This observation proved a strong bonding strength at the

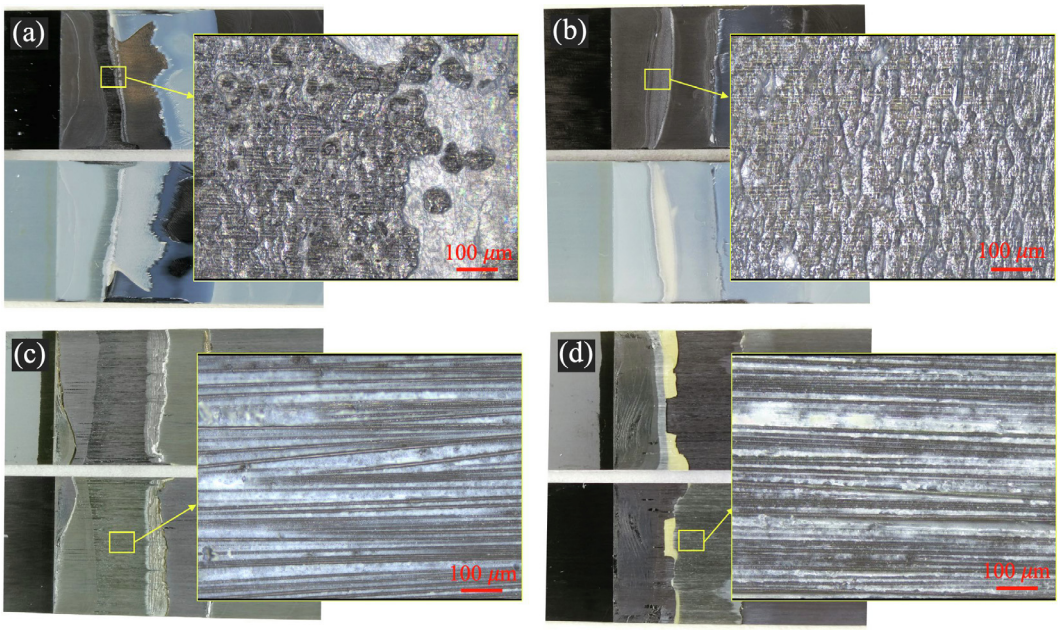

Fig. 13. Representative images of the ENF specimens: (a) and (b) are for the PEEK-CoJoints at 22 °C and 130 °C, respectively; (c) and (d) are for the PEI-CoJoints at 22 °C and 130 °C, respectively.

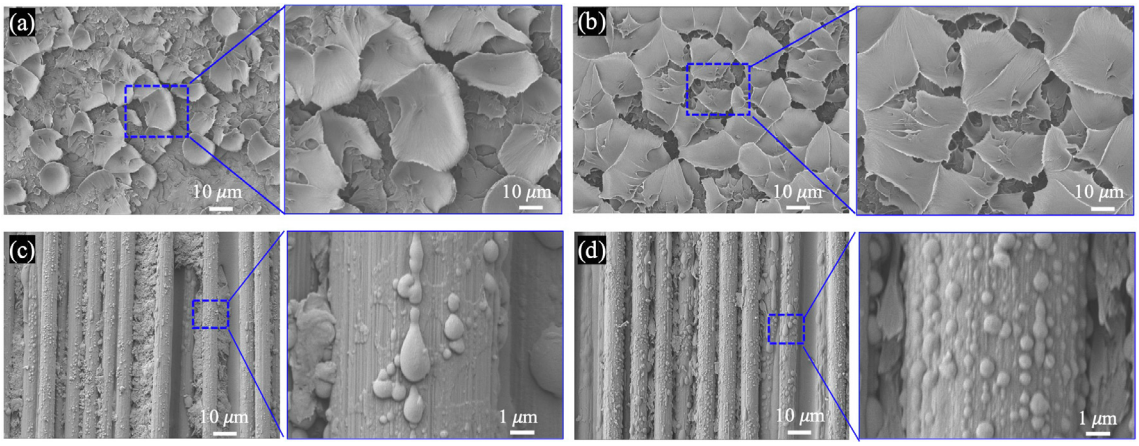

Fig. 14. Representative micrographs of the mode-II fracture surfaces: (a) and (b) are for the PEEK-CoJoints at 22 °C and 130 °C, respectively; (c) and (d) are for the PEI-CoJoints at 22 °C and 130 °C, respectively.

PEEK–epoxy interface within the PEEK-CoJoints. Considering the outstanding mechanical, thermal and fracture properties of PEEK polymer, it is not surprising to see that the PEEK-CoJoints exhibited excellent mode-II fracture resistance at both of 22 °C and 130 °C, see Fig. 11. Fig. 14(c) and (d) show representative SEM micrographs of mode-II fracture surfaces for the PEI-CoJoints. For both of the 22 °C and 130 °C cases, the fracture surfaces of the PEI-CoJoints were characterised with debonded carbon fibres, on which, numerous hemispheric PEI particles were observed. During the mode-II fracture process, these PEI particles served as interlocking pins to prevent carbon fibre debonding, which enhanced the fracture resistance of the PEI-CoJoints under mode-II loading.

4. Conclusions

This study shed light on the development advanced composite joints via a co-cure joining process using high-performance PEEK and PEI films as joining agent. The key to obtain high-performance co-cured joints was to create strong interactions/bonding between the thermoplastic films and the thermosetting (epoxy) matrix of the laminate. This was achieved by carrying out an intensive UV-irradiation to PEEK surfaces for 10 s, while the PEI films possessed naturally good miscibility with the epoxy. Overall, the PEEK-CoJoints exhibited outstanding resistance to both of mode-I and mode-II fracture. In specific, G_{IC} was essentially the same for the PEEK-CoJoints and the aerospace adhesive FM300-CoJoints at 22 °C, while G_{IC} of the PEEK-CoJoints at 130 °C was over 4 times of that of the FM300-CoJoints. Moreover, for both of the 22 °C and 130 °C cases, the mode-II fracture initiation energy of the PEEK-CoJoints was over 2 times of that of the FM300-CoJoints. The fracture resistance of the PEI-CoJoints was not as remarkable as the PEEK-CoJoints, as they possessed much lower G_{IC} than the FM300-CoJoints at 22 °C. Nevertheless, the PEI-CoJoints exhibited a much better mode-II fracture resistance than the FM300-CoJoints in all cases. Overall, the co-cure joining of composite by thermoplastic films had exhibited significant application potentiality in the fabrication, co-cure bonding, strengthening and repairing of integrated composite structures for aerospace industries.

CRediT authorship contribution statement

Dong Quan: Writing – original draft, Investigation, Funding acquisition, Conceptualization. **Yannan Ma:** Investigation, Data curation. **Dongsheng Yue:** Investigation, Data curation. **Jiaming Liu:** Resources, Methodology. **Jun Xing:** Resources, Methodology. **Mingming Zhang:** Visualization, Investigation. **René Alderliesten:** Validation, Resources, Conceptualization. **Guoqun Zhao:** Supervision, Project administration, Funding acquisition.

Declaration of competing interest

The authors declare that they have no known competing financial interests or personal relationships that could have appeared to influence the work reported in this paper.

Data availability

Data will be made available on request.

Acknowledgements

The authors would like to acknowledge the financial support from Natural Science Foundation of Shandong Province, China (Grant No.: 2022HWYQ-013), the key research and development program of Shandong Province, China (Grant No. 2021ZLGX01), and Qilu Young Scholar Program of Shandong University, China (Grant No.: 31370082163164). Dong Quan is grateful to the European Union's Horizon 2020 research and innovation programme under the Marie Skłodowska–Curie grant agreement No. 842467.

References

[1] S. Lu, H. Ding, K. Rong, S. Rong, J. Tang, B. Xing, Composite mechanical deformation based semi-analytical prediction model for dynamic loaded contact pressure of thin-walled aerospace spiral bevel gears, Thin-Walled Struct. 171 (2022) 108794, http://dx.doi.org/10.1016/j.tws.2021.108794.

[2] Y. Zhang, Y. Zhou, Investigation of bird-strike resistance of composite sandwich curved plates with lattice/foam cores, Thin-Walled Struct. 182 (2023) 110203, http://dx.doi.org/10.1016/j.tws.2022.110203.

[3] Y. Liu, W. Zhuang, Y. Luo, D. Xie, W. Mu, Joining mechanism and damage of self-piercing riveted joints in carbon fibre reinforced polymer composites and aluminium alloy, Thin-Walled Struct. 182 (2023) 110233, http://dx.doi.org/10.1016/j.tws.2022.110233.

[4] Z. He, Q. Luo, Q. Li, G. Zheng, G. Sun, Fatigue behavior of CFRP/Al adhesive joints — Failure mechanisms study using digital image correlation (DIC) technique, Thin-Walled Struct. 174 (2022) 109075, http://dx.doi.org/10.1016/j.tws.2022.109075.

[5] H. Jiang, Y. Wang, Y. Ren, Controllable energy-absorption behaviors of the perforated CFRP tube with an adhesively bonded CFRP patch, Thin-Walled Struct. 181 (2022) 110015, http://dx.doi.org/10.1016/j.tws.2022.110015.

[6] L. Jiang, S. Xiao, D. Dong, B. Yang, D. Chen, G. Yang, T. Zhu, M. Wang, Experimental study of bonded, bolted, and hybrid braided CFRP joints with different stacking sequences and lapping patterns, Thin-Walled Struct. 177 (2022) 109408, http://dx.doi.org/10.1016/j.tws.2022.109408.

[7] Z. Wang, C. Li, L. Sui, G. Xian, Effects of adhesive property and thickness on the bond performance between carbon fiber reinforced polymer laminate and steel, Thin-Walled Struct. 158 (2021) 107176, http://dx.doi.org/10.1016/j.tws.2020.107176.

[8] A.J. Kinloch, Adhesion and Adhesives: Science and Technology, Chapman and Hall, 1987.
[9] 3M Website, https://multimedia.3~m.com/mws/media/282041O/3m-scotch-weld-structural-adhesive-film-af-163-2-af-163-3.pdf Last Accessed 29th September 2022.
[10] D. Quan, A. Ivankovic, Effect of core–shell rubber (CSR) nano-particles on mechanical properties and fracture toughness of an epoxy polymer, Polymer 66 (2015) 16–28, http://dx.doi.org/10.1016/j.polymer.2015.04.002.
[11] D. Quan, N. Murphy, A. Ivankovic, Fracture behaviour of a rubber nano-modified structural epoxy adhesive: Bond gap effects and fracture damage zone, Int. J. Adhes. Adhes. 77 (2017) 138–150, http://dx.doi.org/10.1016/j.ijadhadh.2017.05.001.
[12] D. Quan, R.A. Pearson, A. Ivankovic, Interaction of toughening mechanisms in ternary nanocomposites, Polym. Compos. 39 (10) 3482–3496, http://dx.doi.org/10.1002/pc.24368.
[13] J.-H. Back, C. Hwang, D. Baek, D. Kim, Y. Yu, W. Lee, H.-J. Kim, Synthesis of urethane-modified aliphatic epoxy using a greenhouse gas for epoxy composites with tunable properties: Toughened polymer, elastomer, and pressure-sensitive adhesive, Composites B 222 (2021) 109058, http://dx.doi.org/10.1016/j.compositesb.2021.109058.
[14] D. Srinivasan, V. Ravichandran, S. Idapalapati, Failure analysis of GFRP single lap joints tailored with a combination of tough epoxy and hyperelastic adhesives, Composites B 200 (2020) 108255, http://dx.doi.org/10.1016/j.compositesb.2020.108255.
[15] S. Deng, L. Djukic, R. Paton, L. Ye, Thermoplastic/epoxy interactions and their potential applications in joining composite structures - A review, Composites A 68 (2015) 121–132, http://dx.doi.org/10.1016/j.compositesa.2014.09.027.
[16] U. Farooq, S. Heuer, J. Teuwen, C. Dransfeld, Effect of a dwell stage in the cure cycle on the interphase formation in a poly(ether imide)/high tg epoxy system, ACS Appl. Polym. Mater. 3 (12) (2021) 6111–6119, http://dx.doi.org/10.1021/acsapm.1c00956.
[17] D.-P. Turmel, I. Partridge, Heterogeneous phase separation around fibres in epoxy/PEI blends and its effect on composite delamination resistance, Compos. Sci. Technol. 57 (8) (1997) 1001–1007, http://dx.doi.org/10.1016/S0266-3538(96)00148-0.
[18] E. Tsiangou, J. Kupski, S. Teixeira de Freitas, R. Benedictus, I.F. Villegas, On the sensitivity of ultrasonic welding of epoxy- to polyetheretherketone (PEEK)-based composites to the heating time during the welding process, Composites A 144 (2021) 106334, http://dx.doi.org/10.1016/j.compositesa.2021.106334.
[19] E. Tsiangou, S. Teixeira de Freitas, I. Fernandez Villegas, R. Benedictus, Investigation on energy director-less ultrasonic welding of polyetherimide (PEI)- to epoxy-based composites, Composites B 173 (2019) 107014, http://dx.doi.org/10.1016/j.compositesb.2019.107014.
[20] E. Tsiangou, S.T. de Freitas, R. Benedictus, I.F. Villegas, On the sensitivity of the ultrasonic welding process of epoxy- to polyetheretherketone (PEEK)-based composites to the welding force and amplitude of vibrations, Composites C 5 (2021) 100141, http://dx.doi.org/10.1016/j.jcomc.2021.100141.
[21] D. Quan, G. Zhao, G. Scarselli, R. Alderliesten, Co-curing bonding of carbon fibre/epoxy composite joints with excellent structure integrity using carbon fibre/PEEK tapes, Compos. Sci. Technol. 227 (2022) 109567, http://dx.doi.org/10.1016/j.compscitech.2022.109567.
[22] D. Quan, R. Alderliesten, C. Dransfeld, I. Tsakoniatis, S. Teixeira De Freitas, G. Scarselli, N. Murphy, A. Ivankovic, R. Benedictus, Significantly enhanced structural integrity of adhesively bonded PPS and PEEK composite joints by rapidly UV-irradiating the substrates, Compos. Sci. Technol. 199 (2020) 108358, http://dx.doi.org/10.1016/j.compscitech.2020.108358.
[23] D. Quan, B. Deegan, L. Byrne, G. Scarselli, A. Ivankovic, N. Murphy, Rapid surface activation of carbon fibre reinforced PEEK and PPS composites by high-power UV-irradiation for the adhesive joining of dissimilar materials, Composites A 137 (2020) 105976, http://dx.doi.org/10.1016/j.compositesa.2020.105976.
[24] ASTM Standard D5528-13(2013), Standard Test Method for Mode I Interlaminar Fracture Toughness of Unidirectional Fiber-Reinforced Polymer Matrix Composites, ASTM International, 2013.
[25] ASTM Standard D7905/D7905M, Standard Test Method for Determination of the Mode II Interlaminar Fracture Toughness of Unidirectional Fiber-Reinforced Polymer Matrix Composites, ASTM International, 2019.
[26] L. Bonnaud, A. Bonnet, J.P. Pascault, H. Sautereau, C.C. Riccardi, Different parameters controlling the initial solubility of two thermoplastics in epoxy reactive solvents, J. Appl. Polym. Sci. 83 (6) (2002) 1385–1396, http://dx.doi.org/10.1002/app.10029.
[27] I. Mathieson, R. Bradley, Improved adhesion to polymers by UV/ozone surface oxidation, Int. J. Adhes. Adhes. 16 (1) (1996) 29–31, http://dx.doi.org/10.1016/0143-7496(96)88482-X.
[28] B. Blackman, A. Kinloch, M. Paraschi, The determination of the mode II adhesive fracture resistance, G_{IIC}, of structural adhesive joints: an effective crack length approach, Eng. Fract. Mech. 72 (6) (2005) 877–897, http://dx.doi.org/10.1016/j.engfracmech.2004.08.007.
[29] R. Palazzetti, A. Zucchelli, Electrospun nanofibers as reinforcement for composite laminates materials - A review, Compos. Struct. 182 (2017) 711–727, http://dx.doi.org/10.1016/j.compstruct.2017.09.021.